IEEE Access
Multidisciplinary | Rapid Review | Open Access Journal

Received August 6, 2019, accepted August 25, 2019, date of publication September 4, 2019, date of current version September 19, 2019.

Digital Object Identifier 10.1109/ACCESS.2019.2939484

An Efficient FG-FFT With Optimal Replacement Scheme and Inter/Extrapolation Method for Analysis of Electromagnetic Scattering Over a Frequency Band

WEI-BIN KONG[1,4], JIA-YE XIE[3], FENG ZHOU[1,5], XIAO-FANG YANG[1], RU-GANG WANG[1,5], AND KAI-LAI ZHENG[2,4]

[1]College of Information Engineering, Yancheng Institute of Technology, Yancheng 224051, China
[2]National and Local Joint Engineering Laboratory of RF Integration and Micro-Assembly Technology, College of Electronic and Optical Engineering, Nanjing University of Posts and Telecommunications, Nanjing 210023, China
[3]Industrial Center, Nanjing Institute of Technology, Nanjing 211167, China
[4]State Key Laboratory of Millimeter Waves, Southeast University, Nanjing 210096, China
[5]Key Laboratory of Underwater Acoustic Signal Processing, Ministry of Education, Southeast University, Nanjing 210096, China

Corresponding authors: Wei-Bin Kong (kongweibin2007@sina.com) and Feng Zhou (zfycit@ycit.edu.cn)

This work was supported in part by the Natural Science Foundation of China under Grant 61673108 and Grant 11801492, in part by the Natural Science Foundation of the Jiangsu Higher Education Institutions of China under Grant 18KJD510010, Grant 19KJA110002, and Grant 19KJB510061, in part by the Open Research Program of the State Key Laboratory of Millimeter Waves, Southeast University, under Grant K201928, in part by the Open Project Program of the Key Laboratory of Underwater Acoustic Signal Processing, Ministry of Education, under Grant UASP1801, in part by the Fundamental Research Funds for the Central Universities under Grant 2242016K3-0013, in part by the Open Research Program of the National and Local Joint Engineering Laboratory of RF Integration and Micro-Assembly Technology under Grant KFJJ20170306, and in part by the Natural Science Foundation of Jiangsu Province under Grant BK20181050.

ABSTRACT In this paper, the replacement values to the singularity of fitting Green's function are intensively researched in Fitting Green's function Fast Fourier Transformation (FG-FFT) for different frequency points. As is shown in the research, the different replacement values caused the different accuracy of fitting Green's function. The experiments show that an universal appropriate replacement value can improve the accuracy of the fitting Green's function over the entire frequency band, and it is called the optimal wide-band replacement value in this paper. In the case of application of the optimal replacement scheme to FG-FFT, the number of the near correction elements is significantly reduced. Meanwhile, FG-FFT with the proposed scheme and interpolation method herein is used for wide-band analysis of electrically large objects to overcome the obvious error in FG-FFT with traditional replacement scheme and interpolation method. The near correction matrix elements can be interpolated over the entire frequency band with the new scheme, thereby achieving effective combination of the FG-FFT with matrix inter/extrapolation method, which greatly improved the computational efficiency for wide-band analysis.

INDEX TERMS Radar cross sections, Green's function, singularity, FG-FFT, near correction elements.

I. INTRODUCTION

The method of moments (MoM) [1] is an effective tool commonly used in the analysis of electromagnetic scattering or radiation frequency domain problems. Compared with other computational methods, MoM has advantages like high accuracy and good stability. However, the scope of its application is limited due to the high complexity. Meanwhile MoM is difficult to analysis wide-band problem, which is a hot concept and difficult point in electromagnetics scattering. The existing major methods with MoM for analysis wide-band problem can be divided into two categories: methods based on interpolation current, and methods based on interpolation impedance matrix. The first category methods such as asymptotic waveform evaluation (AWE) technique [2], [3], model-based parameter estimation (MBPE) [4]–[6] and skeleton-based wide-band algorithm (SBWBA) [7], have advantages of fast interpolated calculation and easy integration between fast algorithms. However, the equivalent currents are not a linear function of frequency

The associate editor coordinating the review of this article and approving it for publication was Mengmeng Li.

so that great many the frequency samples are required. The second category methods [8]–[13], impedance matrix interpolation methods, have high accuracy and good stability over the entire frequency band.

For the second category methods based on impedance matrix interpolation, direct application of MoM has already been described in papers. However, because of the excessively high storage and computational complexity requirements, its application is greatly limited. The fast algorithms of MoM can effectively reduce the storage requirement and computational complexity [14]–[28]. But for a long time, the combination of the fast algorithms with impedance matrix interpolation methods has encountered great difficulties. For example, when MLFMA is used in the impedance matrix interpolation methods, ''low frequency interruption'' problem will be encountered in the low frequency band. When the traditional FFT-based fast algorithms combine with these category methods, large interpolation error and seriously lowered accuracy are often likely because of cognitive misconception.

In the traditional FFT-based fast algorithms, near elements must be corrected by MoM, that is, near elements must belong to the near correction matrix. The near elements here refer to the elements that intersect the expansion box of basis function and the expansion box of testing function in a unified Cartesian grid. Since boxes intersection inevitably lead to the singularity of fitting Green's function, the traditional FFT-based fast algorithms replace the singularity by a constant, but do not study the replacement value in depth. This paper, in contrast, studies replacement experimental data at first and finds that near elements can still keep high fitting accuracy within a certain range when optimal replacement value is chosen. Near elements within this range can be corrected without using MoM, so this part of near elements will belong to the far matrix. In other words, the new scheme will significantly reduce the number of elements in near correction matrix. Moreover, such characteristic is similar over the entire frequency band. We find that FG-FFT with optimal replacement scheme not only overcomes the problem of inaccurate inter/extrapolation of near matrices by traditional replacement scheme, but also significantly reduces the memory requirement and the computational time compared to the traditional FG-FFT point-by-point calculation. Thus, efficient calculation of wide-band analyzing problem by FG-FFT combined with inter/extrapolation matrix method is achieved.

II. MOM MATRIX INTER/EXTRAPOLATION FORMULA AND FG-FFT

A. INTER/EXTRAPOLATION OF MOM MATRICES

Electric field integral equation (EFIE) is often used to analyze the 3D electromagnetic problems of PEC in free space. After using MoM, the integral equation is transformed into matrix equation.

$$ZI = V \tag{1}$$

where Z, I and V represent the MoM-Matrix, the current coefficients vector, and the excitation vector, respectively. Their elements are all functions of frequency f, whose variation range is $[f_l, f_h]$. The surface of the target is discretized at the highest frequency of f_h. And triangulation is adopted. Wavelength of the highest frequency is denoted by λ_h. Z_{mn} is defined as a matrix element of Z, which needs to be corrected for more accurate interpolation. Element expression of its corrected matrix element is [10]:

$$\tilde{z}_{mn}(f_r) = \begin{cases} z_{mn}(f_r) f_r e^{j2\pi f_r R_{mn}}, & S_m \cap S_n = 0 \\ z_{mn}(f_r) f_r, & S_m \cap S_n \neq 0 \end{cases} \tag{2}$$

here $f_r = f/f_h$ is the normalized frequency. R_{mn} is the distance between facet S_m and facet S_n. $S_m \cap S_n \neq 0$ means that the facets S_m and S_n have at least one common triangle, while $S_m \cap S_n = 0$ means that the facets S_m and S_n have no common triangles. Frequency-sweeping cases by cubic polynomial inter/extrapolation method are utilized [10]. The method firstly calculates the corrected matrices on four normalized frequency points $x_i = f_i/f_h$ $(i = 0, 1, 2, 3)$ by MoM. The Chebyshev interpolation nodes is adopted in this paper. The inter/extrapolation expression for each frequency point f_r in the frequency band $[f_l, f_h]$ is:

$$\tilde{z}_{mn}(f_r) = \sum_{i=0}^{3} \tilde{z}_{mn}(x_i) \psi_i(f_r) \tag{3}$$

where

$$\psi_i(f_r) = \prod_{j=0, j\neq i}^{j=3} \left(\frac{f_r - x_j}{x_i - x_j} \right) \tag{4}$$

In this way, elements of MoM-Matrix on each frequency point can be obtained over the entire frequency band $[f_l, f_h]$ simply by interpolation using Eq. (3). Afterwards, surface current is iteratively calculated, thereby obtaining the RCS over the entire frequency band.

B. FG-FFT

Since MoM requires the high computational complexity and memory requirements, fast algorithms are a necessary means for electrically large targets. Among them, FFT-based fast algorithms are efficient methods. The MoM-matrix Z is approximated as Z^{FFT}, which consists of two parts: Z^{near} and Z^{far} [25]

$$Z = (Z - Z^{far}) + Z^{far} \cong Z^{near} + Z^{far} \triangleq Z^{FFT} \tag{5}$$

here Z^{near} is referred to as the near correction matrix, which is defined as the near part of $\left(Z - Z^{far}\right)$. Computational expression for Z^{far} is:

$$Z^{far} = jk\eta \Pi \cdot G \cdot \Pi^T - j\frac{\eta}{k} \Pi_d \cdot G \cdot \Pi_d^T \tag{6}$$

where η and k are the wave impedance and the wave number in the free space, respectively; Π and Π_d are the coefficient transformation matrices; G is a triple Toeplitz matrix related to the Green's function. The matrix-vector product of $Z^{far} I$

can be sped up by FFT in the FFT-based fast algorithms. Here the Green's function is defined as:

$$G\left(r, r'\right) = \frac{e^{-j2\pi f_r R}}{4\pi R} \tag{7}$$

here r represents the field point; and r' represents the source point.

We note that the far part of Z^{far} in Eq. (5) is the approximation of the far part of Z. In other words, in the far part, $Z \approx Z^{FFT}$. Meanwhile singularity occurs during computation of Green's function in the near part of Z^{far}. To implement numerical calculation, traditional FFT-based fast algorithms replace $R = 0$ with the smaller value R', thereby avoiding singularity in the numerical calculation.

In FG-FFT, the projection coefficients are obtained by solving the following overdetermined equations [25]

$$G(p, r') = \sum_{v \in C_n} \pi^{r'}_{v,C_n} G(p, v) \tag{8}$$

where C_n is the expansion box of r', and p are sample points. The projection coefficients $\pi^{r'}_{v,C_n}$ are to be determined.

C. WIDE-BAND ANALYSIS USING FG-FFT

FG-FFT is efficient in reducing the far-field storage requirements and computational complexity. However, for the near correction matrix of electrically large targets also needs plenty of storage and filling time, since its each element still needs to be calculated independently and stored separately. To avoid repetitive computation of near correction matrix for each frequency point, the near correction matrix should be interpolated by polynomial as Eq. (3). According to Eq. (5), the matrix for normalized frequency f_r after using near correction matrix interpolation scheme is expressed as

$$Z^{FFT}\left(f_r\right) = \left(Z^{near}\right)^{In}\left(f_r\right) + Z^{far}\left(f_r\right) \tag{9}$$

where $(Z^{near})^{In}$ is obtained by cubic polynomial inter/extrapolation method. Here we focus on discussing the near elements. The computational for any near element can be rewritten as

$$Z^{FFT}_{mn}\left(f_r\right) = \left(Z_{mn} - Z^{far}_{mn}\right)^{In}\left(f_r\right) + Z^{far}_{mn}\left(f_r\right) \tag{10}$$

However, experimental data show that in the traditional FG-FFT, Z^{far}_{mn} is always far greater than Z_{mn} in the near field part, so that Z_{mn} is "submerged" by the interpolation error between Z^{far}_{mn} and $\left(Z^{far}_{mn}\right)^{In}$, thus resulting with large error in the near part. This phenomenon is prevalent among FFT-based fast algorithms. To avoid interpolation error in the near part, research and innovation on the near part of FG-FFT is necessary.

III. FITTING SINGULARITY REPLACEMENT SCHEME

In FG-FFT, singularity will appear in the fitting Green's function for near elements, i.e. when the expansion box of field point intersects the expansion box of source point. Traditional approach is to use a smaller value R' instead of $R = 0$ to avoid the singularity in the numerical calculation, followed by correction of the element using MoM. Therefore, in the traditional algorithms, near elements must belong to the near correction matrix. In this section, we first study the effect of different replacement values on the fitting of the near elements. Then an optimal replacement value is obtained by analyzing the experimental data.

A. THE EFFECT OF DIFFERENT REPLACEMENT VALUES AT $F_R = 1$

First, we choose 14 intervals $\left[\frac{h}{2} + \left(\frac{h}{4}\right) \times i, \frac{h}{2} + \left(\frac{h}{4}\right) \times (i+1)\right], i = 0 \cdots 13$ and randomly choose 1000 points in each interval as the distance between field point r and source point r', which is denoted by d. Meanwhile, field point r and source point r' are generated randomly for each distance. Grid spacing for expansion boxes of field point r and source point r' is both h, and the order is both $M = 2$. Starting point of the expansion box C_m of field point r is set as $\left(\left[\frac{r}{h}\right] - 1\right) \times h$, while that of the expansion box r' is set as $\left(\left[\frac{r'}{h}\right] - 1\right) \times h$. Here $[\cdot]$ represents the rounding down operation. Fitting Green's function between r and r' is expressed as:

$$G^F\left(r, r'\right) = \sum_{u \in C_m} \sum_{v \in C_n} \pi^{r}_{u,C_m} G\left(u, v\right) \pi^{r'}_{v,C_n} \tag{11}$$

here coefficients (π^{r}_{u,C_m} and $\pi^{r'}_{v,C_n}$) are both calculated with FG-FFT [25]. v is the Cartesian grid nodes within C_n, whereas u is the Cartesian grid nodes within C_m. When r and r' are very close, their corresponding expansion boxes C_m and C_n intersect each other. That is, $\exists u \in C_m$ and $\exists v \in C_n$ s.t. $R = \|u - v\| = 0$. Singularity will appear in the right side of Eq. (11). To avoid this, traditional FG-FFT often consider that a smaller value R' should be selected instead of $R = 0$ in the calculation of Green's function. However, there is no research about the effect of different replacement values R' on the fitting accuracy of the near elements in other papers. To better distinguish between the influences of different R', relatively large R' and small R' are adopted for separate testing, i.e. $R' = 0.002\lambda$ and $R' = 0.1\lambda$. On these 14000 random distances, the points of fitting Green's function are calculated, meanwhile the points of corresponding accurate Green's function are all set as shown in Fig. 1. The root mean square errors (RMSEs) of partial intervals are recorded in Tab. 1. And RMSE is defined as:

$$RMSE = \sqrt{\frac{1}{K}\sum_{m=1}^{K}\left|RE\left(G^F\left(r_m, r'_m\right) - G\left(r_m, r'_m\right)\right)\right|^2} \tag{12}$$

The following conclusions can be drawn from Fig. 1:

1)Regardless R' is 0.002λ or 0.1λ, completely coincident points between the imaginary parts of fitting values and the imaginary parts of accurate values suggest very high fitting accuracy of the imaginary parts, so the fitting error is mainly from real parts.

2)When $d > 3h$, i.e. when r is distant from r', regardless of smaller replacement value $R' = 0.002\lambda$ or larger one

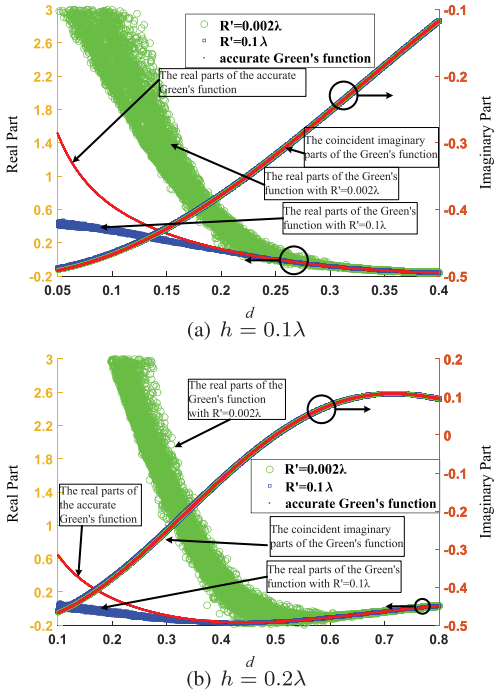

FIGURE 1. The fitting Green's functions and the accurate Green's function.

TABLE 1. RMSEs of the real parts of the fitting Green's functions with $R' = 0.002\lambda$ and $R' = 0.1\lambda$.

d	$h = 0.1\lambda$		$h = 0.2\lambda$	
	$R' = 0.002\lambda$	$R' = 0.1\lambda$	$R' = 0.002\lambda$	$R' = 0.1\lambda$
$[1.25h, 1.5h]$	1.27E+0	1.23E-1	2.04E+0	6.94E-2
$[1.5h, 1.75h]$	8.10E-1	6.50E-2	1.30E+0	3.50E-2
$[1.75h, 2h]$	4.51E-1	3.15E-2	7.24E-1	1.67E-2
$[2h, 2.25h]$	2.20E-1	1.42E-2	3.55E-1	7.64E-3
$[2.25h, 2.5h]$	9.52E-2	6.11E-3	1.56E-1	3.31E-3
$[2.5h, 2.75h]$	3.48E-2	2.27E-3	5.59E-2	1.26E-3
$[2.75h, 3h]$	1.20E-2	8.17E-4	2.01E-2	5.60E-3
$[3h, 3.25h]$	3.25E-3	3.23E-4	5.69E-3	3.13E-4

$R' = 0.1\lambda$, completely coincident points between the real parts of fitting values and the real parts of accurate values suggest that the fitting accuracy of real parts is also very high within this range.

3)When $d < 3h$, the real parts of fitting values separate from the real parts of accurate values for both $R' = 0.002\lambda$ and $R' = 0.1\lambda$, but the degrees and trends are different. Real parts of fitting values corresponding to the smaller replacement value $R' = 0.002\lambda$ are above the real parts of accurate values, while these corresponding to the larger replacement value $R' = 0.1\lambda$ are below the real parts of accurate values.

Through comparisons between the larger and smaller replacement values in Fig. 1 and Tab. 1, we make the following bold speculations:

1)The different replacement values have little influence on the accuracy of imaginary parts of fitting values.

2)Within $d > 3h$, the different replacement values have little influence on the accuracy of real parts of fitting values.

3)Within $d < 3h$, the real parts of fitting values decline gradually from above of real parts of accurate values with increasing R'. So there must be a most appropriate R' which allow the real parts of fitting values to coincide with the real parts of accurate values to the greatest extent. At this time, fitting error of real parts is minimum. At this time R' is called as the optimal replacement value in this paper.

Additionally, it can be found from the figure that the traditional replacement schemes use a relatively small replacement value. For example, when $R = 0$ is replaced by $R' = 0.002\lambda$, the real part of fitting Green's function values is much larger than that of accurate Green's function values.

This leads to the inevitable "submergence" of small number by large number as described in the section II-C under traditional replacement schemes when the interpolation method is adopted for the near correction matrices, thereby resulting in large interpolation error.

B. OPTIMAL REPLACEMENT VALUE WHEN $F_R = 1$

It can be seen from the experiment in section III-A that the imaginary part has high fitting accuracy, so we only need to test the real part of Green's function. Assuming the source point r' is fixed, the field point r is distributed on a circle of radius $R = d$. Here, we consider the case of $f_r = 1$ and $h = 0.1\lambda$. As shown in Fig. 2(a), we compare the three cases

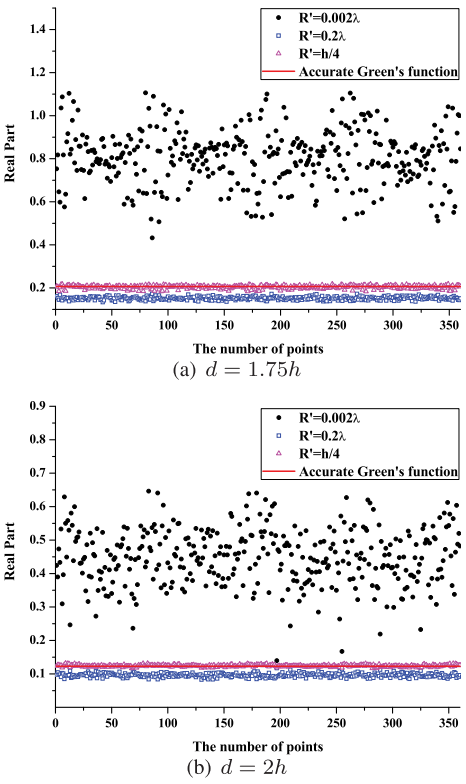

FIGURE 2. The real part of fitting Green's function with different replacement values at $f_r = 1$.

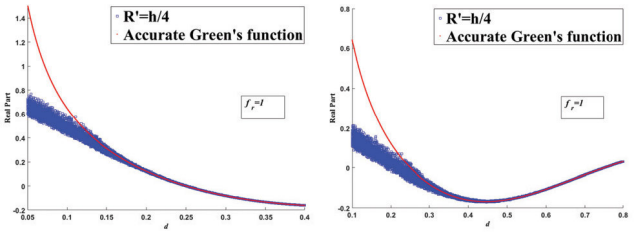

(a) $h = 0.1\lambda$ (b) $h = 0.2\lambda$

FIGURE 3. The real part of fitting Green's function with optimal replacement value and the real part of accurate Green's function at $f_r = 1$.

TABLE 2. RMSEs of the real parts of the fitting Green's functions with optimal replacement value.

d	$h = 0.1\lambda$	$h = 0.2\lambda$
$[1.25h, 1.5h]$	4.34E-2	2.64E-2
$[1.5h, 1.75h]$	1.52E-2	9.06E-3
$[1.75h, 2h]$	5.01E-3	3.45E-3
$[2h, 2.25h]$	2.49E-3	1.76E-3
$[2.25h, 2.5h]$	1.19E-3	1.03E-3
$[2.5h, 2.75h]$	6.70E-4	5.71E-4
$[2.75h, 3h]$	3.94E-4	2.84E-4
$[3h, 3.25h]$	2.31E-4	2.16E-4

of $R' = 0.002\lambda$, $R' = \frac{h}{4}$ and $R' = 0.2\lambda$ at $d = 1.75h$. It can be observed that the fitting accuracy of $R' = \frac{h}{4}$ is the highest and the accuracy remains stable. As shown in Fig. 2(b), the same result is obtained at $d = 2h$.

Therefore, it can be found from the above experiments that $R' = \frac{h}{4}$ is the optimal replacement value. In order to test the effect of optimal replacement value $R' = \frac{h}{4}$ on distance d, the experiment in section III-A is recalculated again. The real parts are presented in Fig. 3, and the fitting errors of the real parts are recorded in Tab. 2.

Through the comparison of Fig. 1 with Fig. 3 and Tab. 1 with Tab. 2, we can draw the following conclusions:

1)Replacement value should not be too large or too small. We demonstrate through a large number of experimental data that $R' = \frac{h}{4}$ is the optimal replacement value for fitting Green's function in the statistical sense. During numerical calculation, we replace $R = 0$ with $R' = \frac{h}{4}$, which allows error minimization of fitting and accurate values of Green's function in the statistical sense.

2)From Tab. 2, we find that the error level is lower than 10^{-3} when $d > 1.75h$ and $R' = \frac{h}{4}$. So presumably the fitting Green's function within this range is approximately equal to the accurate Green's function value and thus does not need correction. Therefore, when the optimal replacement value $R' = \frac{h}{4}$ is applied to the FG-FFT, the element is regarded as the far matrix element if the minimum distance between testing function ψ_m and basis function ψ_n is greater than $1.75h$, otherwise the element is regarded as the near correction matrix element. In this paper, $1.75h$ is called as the threshold between near field and far field. This allows a large number of near elements to be fitted directly without

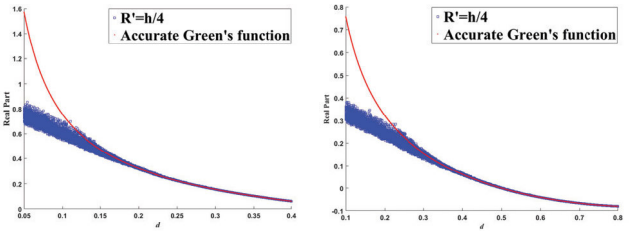

(a) $h = 0.1\lambda$ (b) $h = 0.2\lambda$

FIGURE 4. The real part of fitting Green's function with optimal replacement value and the real part of accurate Green's function at $f_r = 0.5$.

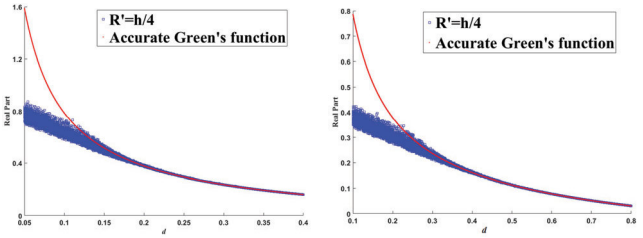

(a) $h = 0\ 1\lambda$ (b) $h = 0\ 2\lambda$

FIGURE 5. The real part of fitting Green's function with optimal replacement value and the real part of accurate Green's function at $f_r = 0.25$.

correction even though they intersect the expansion boxes. In other words, part of near elements no longer belong to the near correction matrix. Hence, the optimal replacement scheme greatly lowers the memory requirements of near correction matrix, thereby reducing the filling time and single iteration time.

C. UNIVERSAL OPTIMAL REPLACEMENT VALUE OVER THE ENTIRE FREQUENCY BAND

The above experiments are about the optimal replacement value obtained at the normalized frequency $f_r = 1$. Whether the optimal replacement value can still maintain small fitting error at other normalized frequencies? We use $R' = \frac{h}{4}$ again, but take two different normalized frequencies $f_r = 0.5$ and $f_r = 0.25$. Comparison between fitting and exact values of Green's function real part is shown in Fig. 4 and Fig. 5, while the fitting errors are recorded in Tab. 3.

We can see from Fig. 4, Fig. 5 and Tab. 3 that $R' = \frac{h}{4}$ remains excellent property under these normalized frequencies. That is, its error level is lower than 10^{-3} in $d > 1.75h$. Through similar experiments with other normalized frequencies, we can also find that the replacement value remains the low error level property on the entire frequency band. Thus $R' = \frac{h}{4}$ is the universal optimal replacement value over the entire frequency band.

Meanwhile, we note that after the use of optimal replacement value, Z_{mn}^{far} and Z_{mn}^{In} are on the same order of magnitude in Eq. (9), or even smaller. This avoids the ''submergence'' of small number by large number as described in section II-C, thereby significantly reducing the interpolation

TABLE 3. RMSEs of the real parts of the fitting Green's functions with optimal replacement value at $f_r = 0.5$ and $f_r = 0.25$.

d	$f_r = 0.5$		$f_r = 0.25$	
	$h = 0.1\lambda$	$h = 0.2\lambda$	$h = 0.1\lambda$	$h = 0.2\lambda$
$[1.25h, 1.5h]$	4.06E-2	2.08E-2	3.99E-2	1.94E-2
$[1.5h, 1.75h]$	1.41E-2	7.04E-3	1.39E-2	6.56E-3
$[1.75h, 2h]$	4.63E-3	2.57E-3	4.54E-3	2.37E-3
$[2h, 2.25h]$	2.26E-3	1.17E-3	2.21E-3	1.06E-3
$[2.25h, 2.5h]$	1.06E-3	6.31E-4	1.03E-3	5.59E-4
$[2.5h, 2.75h]$	5.85E-4	3.23E-4	5.66E-4	2.81E-4
$[2.75h, 3h]$	3.37E-4	1.98E-4	3.24E-4	1.68E-4
$[3h, 3.25h]$	1.93E-4	1.28E-4	1.85E-4	1.05E-4

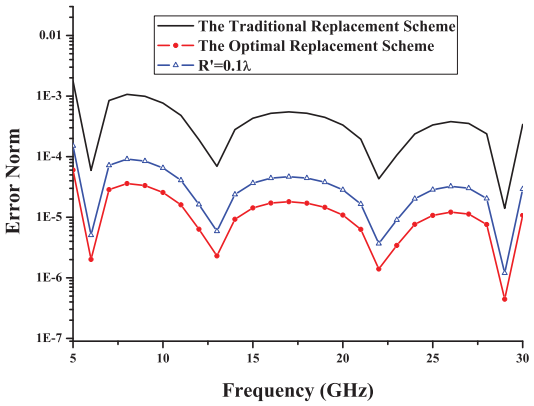

FIGURE 6. The error of self-correction matrix element Z_{11} for the different schemes.

error of near correction matrix. The new scheme realizes accurate polynomial interpolation according to Eq. (9) at any frequency point on the frequency band. In order to verify that the interpolation accuracy of the new scheme is higher than that of the traditional scheme, a numerical example is tested. The PEC sphere with radius of $1\lambda_h$ is considered to illustrate the trend of interpolation accuracy with different replacement values in frequency band. The frequency varies from 5 to 30 GHz. We consider the matrix elements Z_{11}. In Fig. 6, the error norms with different replacement values are plotted. It can be seen that the choice of replacement value has an effect on the interpolation accuracy. Compared with the traditional scheme, the proposed scheme reduces the influence of replacement value on interpolation accuracy.

D. APPLICATION OF UNIVERSAL OPTIMAL REPLACEMENT VALUE TO FG-FFT FREQUENCY SWEEPING

Traditional view holds that singularity will appear during fitting since the expansion box of field point intersects the expansion box of source point in near elements, so that the fitting values will no longer be accurate. Hence, near elements must be corrected by MoM and thus they must belong to the near correction matrix. However, we find through above substantial experiments that the fitting values of near elements can in fact still maintain high accuracy within a considerable interval if optimal replacement value is selected. Firstly, the replacement Green's function is defined:

$$G'(u, v) = \begin{cases} \dfrac{e^{-j2\pi f_r R'}}{4\pi R'}, & R = 0 \\ G, & R \neq 0. \end{cases} \tag{13}$$

here $R = \|u - v\|$, $R' = \frac{h}{4}$. And the Eq. (6) need be rewrite as:

$$Z^{far} = jk\eta\Pi \cdot G' \cdot \Pi^T - j\frac{\eta}{k}\Pi_d \cdot G' \cdot \Pi_d^T \tag{14}$$

Z^{far} in Eq. (14) needs to be calculated directly on each frequency point. We note that G' in Eq. (14) still satisfies the Toeplitz property, so the far matrix Z^{far} can still be computed in an accelerated manner using FFT. Z^{near} is still defined as the near part of $\left(Z - Z^{far}\right)$ in Eq. (5), which is corrected using Eq. (2). The near correction matrices is computed only at four frequency points, followed by interpolation calculation of other frequency points according to Eq. (9). In the optimal replacement scheme, the elements are regarded as near correction matrix elements only when the minimum distance between testing function ψ_m and basis function ψ_n is less than $1.75h$, rather than the traditional basis of whether the expansion boxes intersect. The new scheme significantly reduces the number of elements of Z^{near}.

Meanwhile, the universal optimal replacement value $R' = \frac{h}{4}$ maintains excellent accuracy over the entire frequency band. Besides, it is guaranteed that the near elements in Z^{far} are always smaller than the corresponding ones calculated by MoM. Thus, the "submergence" of small number by large number as described in section II-C encountered during interpolation is avoided. The universal optimal replacement scheme effectively reduces the interpolation error of near correction matrices over the entire frequency band.

Therefore, when FG-FFT with universal optimal replacement scheme is applied to the wide-band analysis of conductor targets, the near correction matrix Z^{near} as a whole is inter/extrapolated with the cubic polynomial, thereby avoiding repetitive computation of near part at each frequency point. Meanwhile, compared to the traditional FG-FFT with point-by-point calculation, FG-FFT with the universal optimal replacement scheme and interpolation method effectively reduces the memory requirements and filling time of near correction matrix and greatly improves the efficiency of frequency sweeping.

IV. NUMERICAL RESULTS

In this section, several numerical examples are provided to verify the computational accuracy and efficiency of FG-FFT with universal optimal replacement scheme for wide-band analysis of conductor target. Grid spacing in the three directions is the same, i.e. $h_x = h_y = h_z = h$, while expansion order is $M = 2$. $\psi_m\,(\psi_n)$ is the testing (basis) function; and $C_m\,(C_n)$ is its expansion box. In the traditional schemes, elements are regarded as near elements when C_m and C_n intersect. In the universal optimal replacement scheme, elements are regarded as near elements when the

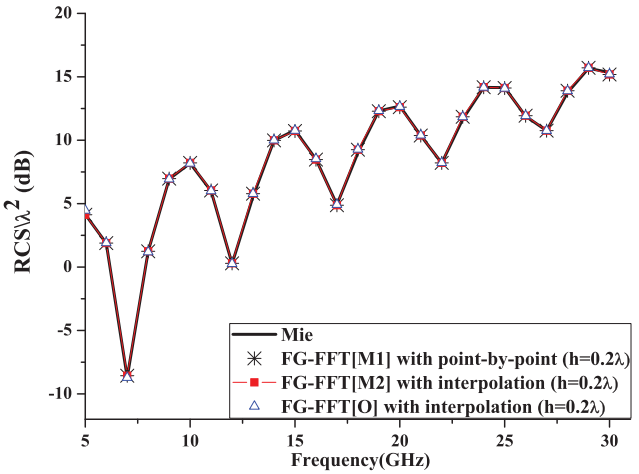

FIGURE 7. The wide-band RCS curves of the PEC sphere.

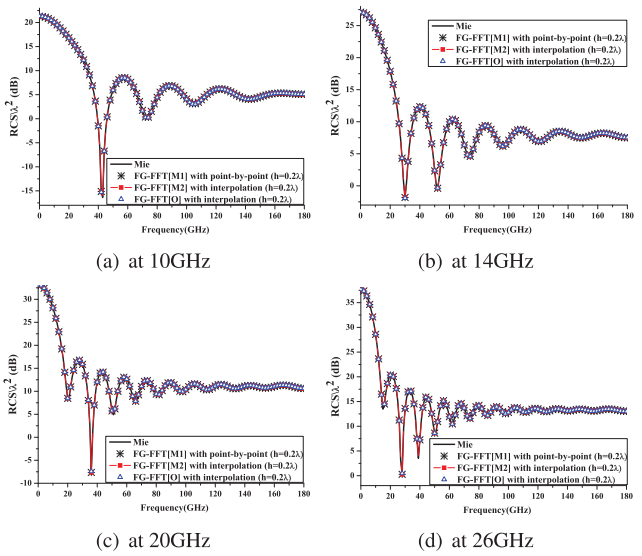

FIGURE 8. The bistatic RCS curves of the PEC sphere.

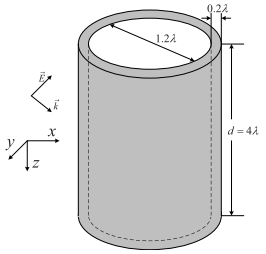

FIGURE 9. A Open cavity.

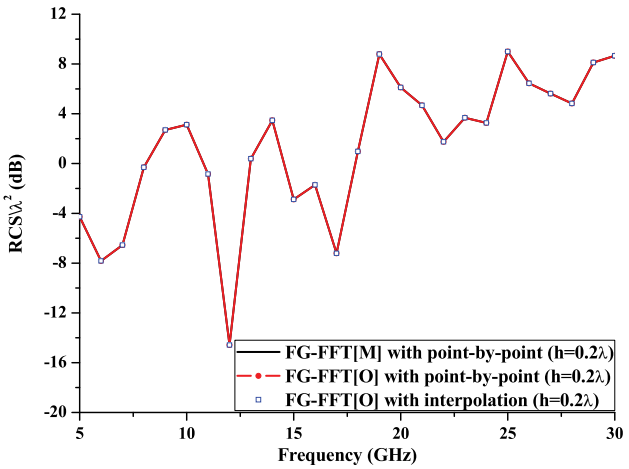

FIGURE 10. The wide-band RCS curves of the PEC open cavity.

minimum distance between ψ_m and ψ_n is less than $1.75h$. We call $1.75h$ the threshold between near field and far field. In the following examples, [M] and [O] represent the traditional replacement scheme and the universal optimal replacement scheme proposed in this paper, respectively. The following examples are all solved using EFIE. The out-of-core memory method is adopted to store the near correction matrixes of four normalized frequencies. All examples use double precision. Computing platform is dual-core eight-thread E3-1505m CPU, while FFT code is from FFTW [29].

A. A PEC SPHERE

A PEC sphere with a radius of $3\lambda_h$ is considered, and the incidence angle of incident plane wave is assumed to be $(\theta^i, \varphi^i) = (0°, 0°)$. Frequency band are selected between [5GHz, 30GHz], and frequency interval is $\Delta f = 1$GHz. The sphere is triangulated with edges $\lambda_h/10$ in length. 40,950 RWG basis functions are generated.

The RCS curves of wide-band are shown in Fig. 7 at scattering angles of $(\theta^s, \varphi^s) = (60°, 0°)$. Fig. 8 illustrates the bistatic RCS curves at 10 GHz, 14 GHz, 20 GHz and 26 GHz, which differ from the interpolated nodes. In Fig. 7 and Fig. 8, computation results of other schemes are compared, of which traditional FG-FFT with point-by-point calculation, and traditional FG-FFT with near correction matrix interpolation. Besides, the analytical results from Mie series are also provided for comparison. FG-FFT with universal optimal replacement scheme interpolation calculation can coincide well with the exact solution RCS curve, suggesting the correctness of the proposed scheme.

B. A PEC OPEN CAVITY

Here, we consider the electromagnetic scattering by a PEC open cavity, as shown in Fig. 9. The direction and polarization of the incident plane wave are also shown in Fig. 9. Here, the depth of the open cavity is $d = 4\lambda_h$. The incidence angle is $(\theta^i, \varphi^i) = (45°, 0°)$. In such cases, the frequency varies from 5 to 30 GHz. The open cavity surface is modeled by with 8,850 triangle patches with the average edge size of $\lambda_h/10$, yielding 13,275 unknowns. The frequency increment of $\Delta f = 1$GHz is considered.

The RCS curves of wide-band are shown in Fig. 10 at scattering angles of $(\theta^s, \varphi^s) = (130°, 0°)$. Plotted in Fig. 10 are the RCS results at the scattering direction obtained

TABLE 4. Some related data at 20 GHz for Example B.

$h(\lambda)$	Method	Memory requirement (M)			CPU time (s)		
		Near-field	Coefficient	Total	Correction matrix	Per iteration	Total
0.2	[M] with point-by-point	172	25	278	49.4	0.32	140
	[O] with point-by-point	67	25	165	19.5	0.27	68
	[O] with interpolation	67	25	165	1.3	0.25	48

TABLE 5. Some related data for Example C.

$h(\lambda)$	Method	Memory requirement (M)			CPU time (s)		
		Near-field	Coefficient	Total	Per Correction matrix	Per iteration	Total
0.1	[M] with point-by-point	195	219	1026	104	9.6	55449
	[O] with interpolation	108	219	938	6	9.4	53289
0.2	[M] with point-by-point	746	192	1035	278	2.5	24932
	[O] with interpolation	304	192	592	18	1.9	13818

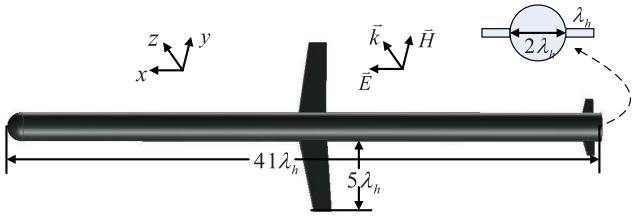

FIGURE 11. A PEC missile-like model.

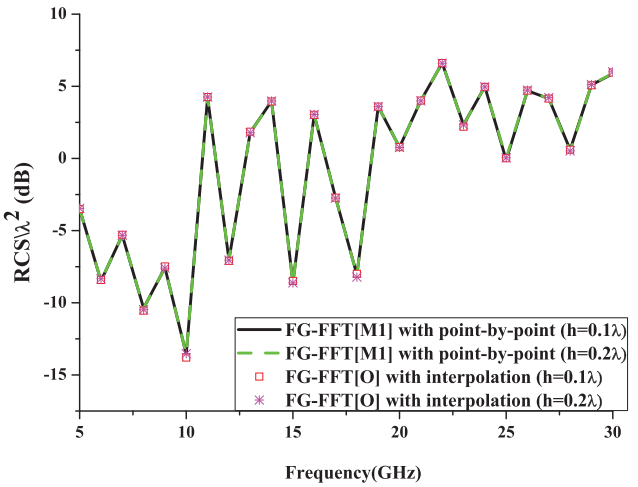

FIGURE 12. The wide-band RCS curves of the PEC missile-like model.

from FG-FFT[M] with point-by-point, FG-FFT[O] with point-by-point, and FG-FFT[O] with interpolation, respectively. It shows that the RCS results computed by FG-FFT[O] with point-by-point and FG-FFT[O] with interpolation agree very well with those by direct FG-FFT[M] with point-by-point. Related data of the three schemes are recorded in Tab. 4. As can be seen, the universal optimal replacement scheme and interpolation method can significantly reduce the memory requirement and the filling time of the near correction matrix, compared with traditional replacement scheme.

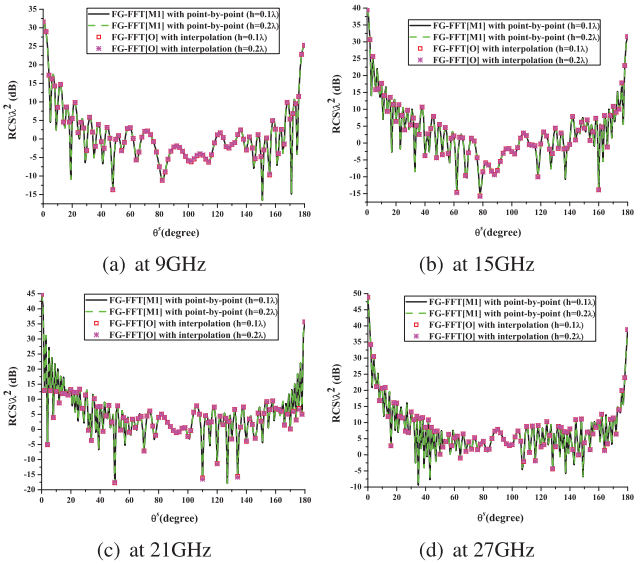

(a) at 9GHz (b) at 15GHz

(c) at 21GHz (d) at 27GHz

FIGURE 13. The bistatic RCS curves of the PEC missile-like model.

C. A PEC MISSILE-LIKE MODEL

A PEC missile-like model is considered in this example, which is shown in Fig. 11. The incidence angle of incident plane wave is assumed to be $(\theta^i, \varphi^i) = (0°, 0°)$. Frequency band is selected between [5GHz, 30GHz], and frequency interval is $\Delta f = 1$GHz. The model is triangulated with edges $\lambda_h/10$ in length. 102,282 RWG basis functions are generated.

The RCS curves of wide-band are shown in Fig. 12 at scattering angles of $(\theta^s, \varphi^s) = (80°, 0°)$. Fig. 13 illustrates the bistatic RCS curves at 9 GHz, 15 GHz, 21 GHz and 27 GHz, which differ from the interpolated nodes. In Fig. 12 and Fig. 13, traditional FG-FFT with point-by-point calculation are compared. The results show that FG-FFT with universal optimal replacement scheme and interpolation method coincides well with the RCS curve of traditional FG-FFT with point-by-point calculation, suggesting the correctness of the proposed scheme again. Related data of the two

schemes are recorded in Tab. 5. As can be seen, the universal optimal replacement scheme and interpolation method can significantly reduce the memory requirement and the filling time of the near correction matrix, compared with traditional replacement scheme. It's important to note that $h = 0.2\lambda$ has the better optimization effect. In this case, the universal optimal replacement scheme reduces the total memory requirement and the total CPU time by about 40% with almost no change in accuracy.

V. CONCLUSION

In this paper, substantial numerical experiments are performed at first to find that different replacement schemes for fitting Green's function singularity have different influences on the fitting accuracy. The universal optimal replacement value over the entire frequency band is sought, which allows the fitting Green's function to be closer to the accurate Green's function value within a certain range, thereby breaking the arbitrariness of replacement values in the traditional FG-FFT. The new replacement scheme can minimize the error of fitting Green's function in the statistical sense and thus greatly reduces the number of near elements in FG-FFT as well as computational time. Besides, the new replacement scheme can avoid the ''submergence'' of small number by large number encountered in the traditional replacement schemes, which can guarantee the accuracy of near correction matrix interpolation over the entire frequency band, thereby achieving effective solving of the wide-band analysis problem of electrically large objects by FG-FFT. Numerical experiments reveal that FG-FFT with universal optimal replacement scheme and interpolation method significantly reduce the memory requirement and the filling time of the near correction matrix, and reduce the total memory requirement and the total CPU time with almost no change in accuracy compared to the traditional FG-FFT with point-by-point calculation for wide-band analysis.

REFERENCES

[1] R. F. Harrington, *Field Computation by Moment Methods*. New York, NY, USA: Macmillan, 1968.

[2] C. J. Reddy, M. D. Deshpande, C. R. Cockrell, and F. B. Beck, "Fast RCS computation over a frequency band using method of moments in conjunction with asymptotic waveform evaluation technique," *IEEE Trans. Antennas Propag.*, vol. 46, no. 8, pp. 1229–1233, Aug. 1998.

[3] A. Setukha and S. Fetisov, "The method of relocation of boundary condition for the problem of electromagnetic wave scattering by perfectly conducting thin objects," *J. Comput. Phys.*, vol. 373, pp. 631–647, Nov. 2018.

[4] E. K. Miller, "Model-based parameter estimation in electromagnetics. III. Applications to EM integral equations," *IEEE Antennas Propag. Mag.*, vol. 40, no. 3, pp. 49–66, Jun. 1998.

[5] Z. Liu, M. Li, G. Zhang, and R. Chen, "Fast broadband analysis of microstrip by interpolating both impedance and preconditioning matrices with MBPE," *Microw. Opt. Technol. Lett.*, vol. 53, no. 8, pp. 1808–1811, Aug. 2011.

[6] L. Li and C.-H. Liang, "Analysis of resonance and quality factor of antenna and scattering systems using complex frequency method combined with model-based parameter estimation," *Prog. Electromagn. Res.*, vol. 46, pp. 165–188, 2004.

[7] X.-M. Pan and X.-Q. Sheng, "Efficient wide-band evaluation of electromagnetic wave scattering from complex targets," *IEEE Trans. Antennas Propag.*, vol. 62, no. 8, pp. 4304–4313, Aug. 2014.

[8] E. H. Newman, "Generation of wide-band data from the method of moments by interpolating the impedance matrix," *IEEE Trans. Antennas Propag.*, vol. AP-36, no. 12, pp. 1820–1824, Dec. 1988.

[9] J. Yeo and R. Mittra, "An algorithm for interpolating the frequency variations of method-of-moments matrices arising in the analysis of planar microstrip structures," *IEEE Trans. Microw. Theory Techn.*, vol. 51, no. 3, pp. 1018–1025, Mar. 2003.

[10] W.-D. Li, H.-X. Zhou, J. Hu, Z. Song, and W. Hong, "Accuracy improvement of cubic polynomial inter/extrapolation of MoM matrices by optimizing frequency samples," *IEEE Antennas Wireless Propag. Lett.*, vol. 10, pp. 888–891, 2011.

[11] W. D. Li, H. X. Zhou, W. Hong, and T. Weiland, "An accurate interpolation scheme with derivative term for generating MoM matrices in frequency sweeps," *IEEE Trans. Antennas Propag.*, vol. 57, no. 8, pp. 2376–2385, Aug. 2009.

[12] P. Du, Y. Shao, and C. Wang, "Fast frequency sweep of metallic antennas using frequency-independent reaction and enhanced gap source model," *J. Electromagn. Waves Appl.*, vol. 31, nos. 11–12, pp. 1093–1100, 2017.

[13] Z. H. Fan, Z. W. Liu, D. Z. Ding, and R. S. Chen, "Preconditioning matrix interpolation technique for fast analysis of scattering over broad frequency band," *IEEE Trans. Antennas Propag.*, vol. 58, no. 7, pp. 2484–2487, Jul. 2010.

[14] H. Zhang, Z. Fan, and R. Chen, "Fast wideband scattering analysis based on Taylor expansion and higher-order hierarchical vector basis functions," *IEEE Antennas Wireless Propag. Lett.*, vol. 14, pp. 579–582, 2015.

[15] L. Wu, Y. Zhao, Q. Cai, R. Zhang, L. Gu, Z. Zhang, and Z. Nie, "MLACE-MLFMA combined with reduced basis method for efficient wideband electromagnetic scattering from metallic targets," *IEEE Trans. Antennas Propag.*, vol. 67, no. 7, pp. 4738–4747, Jul. 2019.

[16] W. Yu, C. Yan, and Z. Wang, "Fast multi-frequency extraction of 3D impedance based on boundary element method," *Microw. Opt. Technol. Lett.*, vol. 50, no. 8, pp. 2191–2197, 2008.

[17] L. Zhao and T. J. Cui, "CG-FFT algorithm for EM scattering by small dielectric particles with high permittivity and permeability," *Microw. Opt. Technol. Lett.*, vol. 49, no. 2, pp. 305–310, Feb. 2007.

[18] H.-L. Sun, C.-M. Tong, and P. Peng, "Analysis of scattering from composite conductor and dielectric objects using single integral equation method and MLFMA based on JMCFIE," *Prog. Electromagn. Res. M*, vol. 52, pp. 141–152, 2016.

[19] L. Ma, Z. Nie, J. Hu, and S. He, "Combined MLFMA—ACA algorithm application to scattering problems with complex and fine structure," in *Proc. Asia Pacific Microw. Conf.*, Singapore, Dec. 2009, pp. 802–805.

[20] X.-M. Pan, J.-G. Wei, Z. Peng, and X.-Q. Sheng, "A fast algorithm for multiscale electromagnetic problems using interpolative decomposition and multilevel fast multipole algorithm," *Radio Sci.*, vol. 47, no. 1, pp. 1–11, Feb. 2012.

[21] M. Li, M. A. Francavilla, F. Vipiana, G. Vecchi, Z. Fan, and R. Chen, "A doubly hierarchical MoM for high-fidelity modeling of multiscale structures," *IEEE Trans. Electromagn. Compat.*, vol. 56, no. 5, pp. 1103–1111, Oct. 2014.

[22] J. Ling, S. Gong, S. Qin, W. Wang, and Y. Zhang, "Wide-band analysis of on-platform antenna using MoM-PO combined with Maehly approximation," *J. Electromagn. Waves Appl.*, vol. 24, no. 4, pp. 475–484, 2010.

[23] S. M. Seo and J.-F. Lee, "A fast IE-FFT algorithm for solving PEC scattering problems," *IEEE Trans. Magn.*, vol. 41, no. 5, pp. 1476–1479, May 2005.

[24] M. Li, R. S. Chen, H. Wang, Z. Fan, and Q. Hu, "A multilevel FFT method for the 3-D capacitance extraction," *IEEE Trans. Comput. Aided Design Integr.*, vol. 32, no. 2, pp. 318–322, Feb. 2013.

[25] J.-Y. Xie, H.-X. Zhou, W. Hong, W.-D. Li, and G. Hua, "A novel FG-FFT method for the EFIE," in *Proc. Int. Conf. Comput. Problem-Solving (ICCP)*, Leshan, China, Oct. 2012, pp. 111–115.

[26] A. Karwowski and A. Noga, "On the interpolation of the frequency variations of the MoM-PO impedance matrix over a wide bandwidth," *Microw. Opt. Technol. Lett.*, vol. 50, no. 3, pp. 738–741, Mar. 2008.

[27] F. Zhou, R. Wang, and J. Bian, "Robust destination jamming aided secrecy precoding for an AF MIMO untrusted relay system," *Wireless Commun. Mobile Comput.*, vol. 2013, May 2019, Art. no. 1081682.

[28] R. Wang and F. Zhou, "Physical layer security for land mobile satellite communication networks with user cooperation," *IEEE Access*, vol. 7, pp. 29495–29505, 2019.

[29] M. Frigo and S. G. Johnson, "The design and implementation of FFTW3," *Proc. IEEE*, vol. 93, no. 2, pp. 216–231, Feb. 2005.

WEI-BIN KONG received the B.S. degree in mathematics from Qufu Normal University, China, in 2007, and the M.S. degree in mathematics and the Ph.D. degree in radio engineering from Southeast University, Nanjing, China, in 2010 and 2015, respectively.

Since 2016, he has been a Lecturer with the College of Information Engineering, Yancheng Institute of Technology, Yancheng. His current research interests include the IE-based domain decomposition methods, the FFT-based fast algorithm, and the hybrid algorithm for multiscale EM problems.

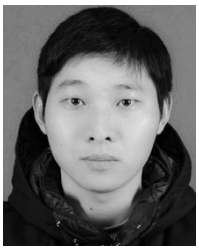

JIA-YE XIE was born in Anhui, China, in 1980. He received the B.S. degree in mathematics from Anhui University, and the M.S. degree in mathematics and the Ph.D. degree in radio engineering from Southeast University.

Since 2018, he has been an Associate Professor with the Industrial Center, Nanjing Institute of Technology, Nanjing, China. His current research interests include the fast algorithms in computational EM and the higher order method of moments.

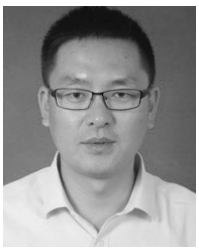

FENG ZHOU received the B.S. and M.S. degrees from Southeast University, Nanjing, China, in 2004 and 2012, respectively. He is currently pursuing the Ph.D. degree with the Army Engineering University of PLA.

Since 2017, he has been an Associate Professor with the College of Information Engineering, Yancheng Institute of Technology, Yancheng, China. His research interests include cooperative communication, satellite communication, cognitive radio, and physical layer security.

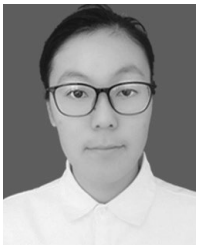

XIAO-FANG YANG received the B.S. and M.S. degrees from Jiangsu Normal University, Xuzhou, China, in 2009 and 2012, respectively, and the Ph.D. degree from Fudan University, Shanghai, China, in 2016, all in optics.

Since 2016, she has been a Lecturer with the College of Information Engineering, Yancheng Institute of Technology, Yancheng, China. Her current research interests include the fiber sensors, computational optics, and optoelectronic information processing.

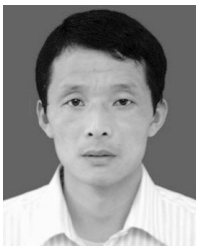

RU-GANG WANG received the B.S. degree from the Wuhan University of Technology, Wuhan, China, in 1999, the M.S. degree from Jinan University, Guangzhou, China, in 2007, and the Ph.D. degree from Nanjing University, Nanjing, China, in 2012.

Since 2012, he has been an Associate Professor with the College of Information Engineering, Yancheng Institute of Technology, Yancheng, China. His research interests include the optical communication networks, novel and key devices for optical communication systems, and computational optics.

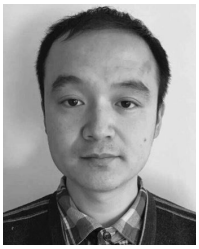

KAI-LAI ZHENG received the B.S. degree in information engineering from Zhengzhou University, Zhengzhou, China, in 2006, and the M.S. and Ph.D. degrees from the State Key Laboratory of Millimeter Waves, Southeast University, Nanjing, China, in 2010 and 2015, respectively.

Since 2015, he has been a Lecturer with the School of Electronic Science and Engineering, Nanjing University of Posts and Telecommunications, Nanjing. His current research interests include numerical algorithms in computational electromagnetics, IE-based domain decomposition methods, and FEM-BI-based domain decomposition methods.